Impacts of continuous inflow of low concentrations of silver nanoparticles on biological performance and microbial communities of aerobic heterotrophic wastewater biofilm

Sanaz Alizadeh[1], Arshath Abdul Rahim[2], Bing Guo[2], Jalal Hawari[1], Subhasis Ghoshal[2], Yves Comeau[1]

[1]Department of Civil, Geological and Mining Engineering, Polytechnique Montreal, 2500 Polytechnique road, Montreal (Quebec) Canada H3T 1J4

[2] Department of Civil Engineering, McGill University, 817 Sherbrooke Street West, Montreal (Quebec) Canada H3A 0C3

Abstract

In this study, two bench-scale moving bed biofilm bioreactors (MBBRs), achieving soluble organic matter removal, were exposed to 10.9 and 109 μg/L polyvinylpyrrolidone (PVP)-coated AgNPs for 9 weeks (64 d). Distribution of continuously added AgNPs were characterized in influent, bioreactor and effluent of MBBRs using single-particle inductively coupled plasma mass spectroscopy (spICP-MS). Continuous exposure to both $AgNP_{inf}$ concentrations significantly decreased soluble chemical oxygen demand (S_{COD}) removal efficiency (11% to 31%) and reduced biofilm viability (8% to 30%). Specific activities of both intracellular dehydrogenase (DHA) and extracellular α-glucosidase (α-Glu) and protease (PRO) enzymes were significantly inhibited (8% to 39%) with an observed NP dose-dependent intracellular reactive oxygen species (ROS) production and shift in biofilm microbial community composition by day 64. The release of significant mass of Ag via effluent (<78%), dominantly in NP form due to the limited retention capacity of aerobic heterotrophic biofilm, provide new and useful insight into fate of AgNPs in biofilm-laden engineered biological systems and their corresponding inhibitory effects at environmentally representative NP concentrations maintained over an extended period. To our knowledge, this is the first study evaluating chronic inhibitory effect of AgNPs on attached-growth wastewater process efficiency and its microbial communities at representative environmental AgNP concentrations by combining biological response and NP characterization.

1. Introduction

Engineered nanoparticles (ENPs) are manufactured at an estimated rate of 11.5 million tons per year for various industrial and commercial applications[1]. Silver nanoparticles (AgNPs) are predominantly used as antimicrobial agents in commercial products, cosmetics, food processing and water industries[1]. This rapidly developing nanotechnology market, however, is leading to their environmental exposure, with a significant fraction of the AgNP-laden domestic and industrial waste streams being released in municipal water resource recovery facilities (WRRFs) at an estimated influent concentration ranging from 10 ng/L to 1.5 μg/L[2-4]. Thus, WRRFs serve as a key interface between ENPs releases and their environmental distribution into downstream ecosystems. Previous studies on the inhibitory effects of AgNPs (0.1 to 50 mg/L) in suspended-growth systems showed adverse effects on the biological performance and biomass activity caused by oxidative stress, cell membrane damage and inactivation of key enzymes at sufficient AgNP doses (< 1 mg/L)[5-9]. Yet, the interaction between biofilm processes and ENPs including AgNPs are poorly understood.

Attached growth processes, such as moving bed biofilm reactors (MBBRs), are commonly used as an upgrade or replacement for existing biological processes to meet current and new effluent discharge requirements, while minimizing plant footprint and operating costs[10,11]. In 2014, more than 1200 WRRFs in at least 50 countries utilize the MBBR technology in both the municipal and industrial sectors with over 36 in North America[12,13]. A limited number of studies investigated the impact of a single dose of AgNPs (1 to 200 mg/L) over 24 to 96 h, using mono-species biofilms, particularly *P. putida* based biofilms or wastewater biofilms in simplified biological media[11,14-16]. Their findings indicated higher potential of biofilm bacteria than planktonic bacteria to withstand the toxic effects of AgNPs, primarily due to the presence of extracellular polymeric substances (EPS), the primary components of biofilm[15], which act to reduce AgNP diffusion in

biofilms[17] over short term exposure conditions. Yet, the results of short-term exposure studies may fail to capture the effects of the expected accumulation of AgNPs and higher mass transport of AgNPs by diffusion into deeper layers of the biofilm over extended time intervals, thus underestimating the potential toxicity of AgNPs over long-term exposure scenarios[18,19]. Further research is thus required first, to understand the interaction mechanisms between ENPs and mature, mixed culture wastewater biofilms and second, to investigate the corresponding AgNP-induced inhibitory effects at environmentally representative NP concentrations under conditions that are representative of typical WRRF processes.

Rigorous physical and chemical characterization of AgNPs combined with extensive biological and toxicological evaluations in WRRFs are critical in laying the grounds for a better understanding of their environmental fate and for the design of better alternative treatment strategies and future regulations[20]. The current understanding of the environmental fate and transformation of ENPs is limited due to the limitations of ENP characterization techniques in complex environmental matrices containing ENPs at very low, environmentally relevant concentrations[21,22]. Single-particle inductively coupled plasma–mass spectrometry (spICP-MS) is an emerging powerful technique with the potential to address such limitations, providing quantitative characterization of metal NP size distributions, particle number concentrations and dissolved metal concentrations at low NPs concentrations in complex, organic matter-rich, environmental matrices such as wastewaters[23-25].

In this study, we investigated the impact of continuous injection of low concentrations of AgNPs in an attached growth wastewater treatment process using aerobic heterotrophic wastewater biofilms at nominal influent concentrations of 10.9 and 109 μg/L AgNPs to approximate environmentally relevant concentrations of AgNPs. Although, these concentrations would still be

at the higher end of the estimated concentration for WRRFs, they would mimic a worst case scenario such as release from biosolid-treated soil or landfills by flooding events or production plant discharge[26]. The specific objectives of this study were (1) to characterize the interactions and distribution of AgNPs in a biofilm-laden wastewater biological process and (2) to determine the impact of AgNPs on primary biological functions and microbial community of wastewater biofilms. Two bench-scale MBBRs were operated for organic matter removal and were fed with a synthetic soluble influent representative of a municipal wastewater. The impacts of AgNPs on the performance of the MBBRs were characterized by monitoring several performance indicators including S_{COD} removal efficiency, effluent quality and enzymatic activity over a 9-week (64 d) exposure period.

The biological responses of aerobic heterotrophic biofilm were characterized in terms of (i) biofilm cell membrane integrity using DNA-binding stains, (ii) AgNP-mediated oxidative stress via intracellular ROS measurement and (iii) microbial metabolic functions by intracellular DHA and extracellular α-Glu and PRO specific enzymatic activities using colorimetric assays. The biofilm microbial community compositions, at both influent AgNPs concentrations, were characterized through high-throughput sequencing. The aggregation state, dissolution and distribution of AgNPs were determined between different reactor components (i.e. influent, bioreactor and effluent) using spICP-MS techniques and transmission electron microscopy with energy dispersive X-ray spectroscopy (TEM EDS). To the best of our knowledge, this is the first study evaluating the long-term inhibitory effect of AgNPs on attached-growth wastewater process efficiency and its microbial communities at environmentally relevant AgNP concentrations (< 100 μg/L AgNPs) by combining biological responses and the NP distribution, characterization and Ag speciation data.

2. Methods

2.1 Reactor configuration and AgNPs exposure

Two 1 L bench-scale MBBRs, achieving organic matter removal at a hydraulic retention time (HRT) of 3 hours, operated in parallel under identical conditions, were fed a synthetic soluble influent (Table S1) to ensure constant influent characteristics and well-controlled conditions to characterize the inhibitory effects of the PVP-AgNPs. The concentrated synthetic wastewater (1.3 ± 0.2 g S_{COD}/L) was pumped and diluted with tap water before entering the reactors to obtain an influent COD concentration of 655 ± 6 mg S_{COD}/L at an organic loading rate of 11 ± 0.2 g COD m^{-2} d^{-1} of active surface area to be representative of the soluble fraction of a medium to high strength domestic wastewater with typical COD/TKN/TP ratio of 100/12.0/2.0[27]. The characteristics of the synthetic influent (Table S2) and detailed reactor operation conditions are presented as supplementary information (SI). After reaching quasi steady-state conditions with a stable S_{COD} removal efficiency, the reactors were monitored for 85 days as a control period. Influent AgNP suspensions were prepared by dilution of 50 nm PVP-coated AgNPs stock suspension (4.73 mg/mL, Nanocomposix Inc., San Diego, US) in Milli-Q water. The zeta potential and surface area of AgNPs were -37.8 mV (at pH 4) and 9.8 m^2/g, respectively, based on the AgNP product description, with a mean diameter of 48 ± 2 nm (SpICP-MS, PerkinElmer NexION 300X). The AgNP influent suspensions were pumped to each reactor from day 125 at a constant flow rate (2.7 ± 0.1 mL/min), resulting in an average influent total Ag concentration of 14 ± 0.5 μg/L Ag for $MBBR_1$ and 130 ± 14 μg/L Ag for $MBBR_2$ after dilution. The influent nanoparticle suspensions were replenished every 24 h. The effluent water quality, biofilm biological responses (e.g. viability or enzyme activity) and Ag distribution were monitored over 64 days. Chemical oxygen demand (COD), total suspended solids (TSS) and volatile suspended solids (VSS) were measured according to Standard Methods[28].

122 **2.2 Silver analyses**

123 The influent, bioreactor and effluent were sampled every 24 h over the first week (day 125-130)
124 and every 3 days afterwards (day 133-189) for a total period of 9 weeks (Figure S1). Bioreactor
125 and effluent samples contained suspended flocs (145 to 480 mg TSS/L) but no K5 carriers. Total
126 Ag concentration was measured in acid-digested homogenized samples using a PerkinElmer
127 NexION 300x ICP-MS in standard mode as described in our previous study[19]. The homogenized
128 samples were allowed to settle for about 30 to 45 s and the aqueous supernatant was collected.
129 AgNP concentration and size as well as dissolved Ag were determined simultaneously using
130 spICP-MS, supported by Syngistix nano application module (version 1.1) as described by Azodi
131 et al.[23]. Instrumental and data acquisition parameters of the analysis are indicated in SI (Table
132 S3). A cumulative Ag mass distribution in influent ($M_{Ag,\ inf}$), bioreactor ($M_{Ag,bio}$) and effluent (
133 $M_{Ag,eff}$) of each MBBR was calculated based on the corresponding total Ag concentrations,
134 obtained from ICP-MS analysis, influent and effluent flow rates, and volume of the bioreactor
135 for each time interval (Δt) as described in our previous study[19]. Ag fractionation and the detailed
136 equations and Ag mass balance are presented in SI.

137 **2.3 Viability and key enzymatic activities of attached biofilm**

138 Bacterial viability of attached biofilms was evaluated using the Live/Dead *Baclight* bacterial
139 viability kit (Molecular Probes, Invitrogen, Kit L13152) and a micro plate reader (Synergy-HT,
140 BioTek, USA) as described by Chen et al.[29]. The specific activities of DHA, α-Glu and PRO
141 enzymes were measured by a colorimetric method[30,31] using 0.5% 2-(4-iodophenyl)-3-(4-
142 nitrophenyl)-5-phenyl-2H-tetrazolium chloride (INT), 1% *p*-nitrophenyl α-D-glucopyranoside
143 and 0.5% azocasein, respectively, as a substrate for the reactions. The intracellular ROS
144 production, as an indicator of oxidative stress, was determined using dichlorodihydrofluorescein

diacetate (H_2DCF-DA, Molecular Probes, Invitrogen)[32]. H_2-DCFDA was used as a cell-permeant reagent that measures hydroxyl, peroxyl and other reactive oxygen species activity in cells. Details regarding all enzyme activity and ROS assays are provided in SI.

2.4 DNA Extraction, sequencing and microbial community analysis

Biofilm samples were collected from $MBBR_1$ and $MBBR_2$ at the end of the control period ($MBBR_1^C$, $MBBR_2^C$) and after exposure to AgNPs for 64 days ($MBBR_1^{64}$, $MBBR_2^{64}$). For each set of the microbial community data, 10 carriers were selected randomly from each reactor; the retained biofilm was homogenized and used for DNA extraction. Genomic DNA was extracted from the biofilm samples using FastDNA®spin kit (MP Biomedicals, Santa Ana, CA) following the manufacturer's instructions, and sent for library preparation and sequencing on the Illumina Miseq PE250 platform at McGill University and Génome Québec Innovation Centre (Montréal, Québec). Bacterial universal primers 515F (5′-GTGCCAGCMGCCGCGGTAA-3′) and 806R (5′-GGACTACHVGGGTWTCTAAT-3′) were used to amplify the V4 variable region of the 16S rDNA. Bioinformatics analysis was performed using QIIME2 pipelines. The de-multiplexed forward and reverse sequences were quality-filtered using DADA2[33] at 100% sequence similarity. Taxonomy was assigned using the 99% operational taxonomic unit (OTU) similarity in the GreenGenes reference database. Alpha-diversity, beta-diversity and their statistical tests were analyzed in QIIME2. Principal coordinates analysis (PCoA) was constructed using weighted UniFrac distance matrix. Heatmap was generated in R using the "gplots" package.

2.5 Statistical analysis

The statistical significance of differences between treatments ($p < 0.05$), before and after exposure to AgNPs, was evaluated with one-way repeated measures ANOVA using Statistica version 12 (StatSoft Inc., USA).

3. Results and discussion

3.1 Fate of AgNPs in MBBRs over 64 days

The influent of $MBBR_1$ and $MBBR_2$ contained an average concentration of 10.9 ± 1.6 μg/L AgNP ($[AgNP_{inf}]$) and 109.3 ± 10 μg/L $AgNP_{inf}$, with mean diameter (d_{mean}) of 49 ± 7 nm and 48 ± 2 nm, respectively, (Figure S2D), corresponding to a total Ag concentration ($[Ag_{inf}]$) of 14 ± 2 μg/L Ag 130 ± 14 μg/L Ag in corresponding reactors (Figure 1A, B). Each of these quantities was independently measured by spICP-MS and ICP-MS. SpICP-MS analyses showed less than 10% variation in dissolved Ag concentrations($[\text{dissolved } Ag_{inf}]$), in influent NP stock solutions of both reactors over time (Figure S2A, B). Three distinct trends (Phases) were observed for Ag concentration profiles in both reactors over the 64-day Ag loading (Figure 1A, B). Phase I corresponded to the first 15 days of AgNP loading (day 125-140) during which both reactors accumulated Ag in response to the AgNP addition and reached a relatively stable Ag retention efficiency (61% to 72% of $[Ag_{inf}]$). A major fraction of the released total silver ($[Ag_{eff}]$) (40% to 63%) was associated with total suspended solids in effluent (TSS_{eff}) in MBBRs. Effluent Ag concentration as NP ($AgNP_{eff}$) in $MBBR_1$ (0.2 to 1.4 μg/L) and $MBBR_2$ (2.9 to 5.5 μg/L) corresponded to approximately $10\% \pm 3\%$ of $[Ag_{eff}]$ and $16\% \pm 4\%$ of $[Ag_{eff}]$, respectively, over Phase I. SpICP-MS analyses showed variations in $[\text{dissolved } Ag_{eff}]$ in the effluent supernatant of $MBBR_1$ (0.2 to 2.6 μg/L) and $MBBR_2$ (4.7 to 11.9 μg/L) representing about 16% to 49% of $[Ag_{eff}]$ as Ag^+ partially or completely complexed to dissolved organic carbon (DOC) (Figure 1A, B). High concentration of dissolved oxygen (6 ± 0.2 mg/L) and pH of 7.2-7.5 in the MBBRs provided thermodynamically favorable conditions for oxidation driven dissolution of AgNPs. Generally, the mean diameter of $AgNP_{eff}$ was up to 7 nm smaller than $AgNP_{inf}$, despite the minor aggregation over 3 initial days of exposure (Figure 1C).

191 The magnitude of change in the diameters was small because of the short average residence time
192 of the AgNPs in the reactor. The particle size distribution of $AgNP_{eff}$ had slightly higher
193 concentrations of smaller particles compared to $AgNP_{inf}$ (Figure S3). The relatively high amount
194 of $[\text{dissolved } Ag_{eff}]$ on certain days (e.g., day 133 in $MBBR_1$ and day 154 in $MBBR_2$) cannot be
195 accounted for the changes in particle diameters in the effluent. It is likely that detachment and
196 release of soluble complexes Ag from the biofilm/EPS matrix resulted in relatively high fraction
197 of $[\text{dissolved } Ag_{eff}]$ relative to $[Ag_{eff}]$. The attached biofilm ($Ag_{carrier}$) retained about 60% to 71%
198 of cumulative mass of total Ag loading in the influent ($M_{Ag_{inf}}$) in $MBBR_1$ (0.88 mg Ag/m^2 of
199 carrier active surface) and $MBBR_2$ (10.3 mg Ag/m^2 of carrier active surface) by the end of
200 Phase 1 (day 140), indicating an initial high Ag biofilm retention capacity (Figure 1D, E). The
201 carrier active surface area represents the biofilm covered surface area.

202 Phase II started with a gradual increase of $[Ag_{eff}]$ which reached a maximum concentration of 8.9
203 ± 1.7 μg/L Ag in $MBBR_1$ and 118.6 ± 1.5 μg/L Ag in $MBBR_2$ over 10 days (day 140 - 150)
204 decreasing the Ag retention efficiency significantly ($p < 0.05$) compared to Phase I due to
205 biofilm detachment (Figure S5). A larger fraction of $[Ag_{eff}]$ (20% to 37%) was detected as NPs
206 in the effluent supernatant of $MBBR_1$ (8.9 to 11.2 μg/L) and $MBBR_2$ (9.02 to 26.5 μg/L). The
207 $[\text{dissolved } Ag_{eff}]$ in $MBBR_1$ and $MBBR_2$ represented about 22% ± 3% of $[Ag_{eff}]$ (1.3 to 3.04
208 μg/L) and 25% ± 8% of $[Ag_{eff}]$ (11.9 to 25.30 μg/L) respectively, in this phase (Figure 1A, B).
209 By the end of Phase II (day 150), the attached biofilm retained only about 44% to 54% of
210 cumulative $M_{Ag_{inf}}$ in MBBRs (Figure 1D, E), followed by a continuous decrease in retention
211 efficiency (Figure 1A, B). The virgin surface of the biofilm retained much AgNPs during Phase
212 I, likely due to interactions of hydrophobic PVP coatings of AgNPs with heterogeneous

amphiphilic moieties of the biofilm surface[34]. As the concentration of AgNPs increased inside the reactors during Phase II, the local accumulation of PVP-AgNPs on the outer layer of the biofilm must have blocked further deposition of AgNPs and caused decrease in NPs attachment efficiency onto the biofilm surface[34].

Phase III corresponded to the period with Ag release and retention recovery events in both reactors (day 154 - 189). The Ag distribution profile in $MBBR_1$ consisted of two Ag release events on day 154 (week 4) and day 164 (week 6) with the $[AgNP_{eff}]$ (9.9 ± 1.7 μg/L to 14.03 ± 0.7 μg/L) constituting 61% to 87% of detected $[Ag_{eff}]$ (Figure 1A, C). Despite a slight Ag recovery in retention by biofilm by day 175 (week 7), significantly higher $[Ag_{eff}]$ were released over the last two weeks of exposure, predominantly in the form of AgNPs (81% to 96% of $[Ag_{eff}]$) likely due to saturation of biofilm outer layers by AgNPs and/or biofilm sloughing off from the surface of the carriers. $MBBR_2$ demonstrated a lower recovery for Ag retention over a longer time interval as compared to $MBBR_1$ during the Phase III. A maximum Ag release of 229 μg/L Ag_{eff} was observed at the beginning of Phase III (day 154) in $MBBR_2$, with a dominant fraction of $[Ag_{eff}]$ detected as $AgNP_{eff}$ (52% of $[Ag_{eff}]$) and dissolved Ag_{eff} (45% of $[Ag_{eff}]$) in the aqueous phase of the effluent (Figure 1B), suggesting a saturation of the biofilm outer layers. Thereafter, $[AgNP_{eff}]$ (80 to 104 μg/L) represented an average 40% to 65% of $[Ag_{eff}]$ between day 161 and day 189 (Figure 1B). A relatively smaller mass fraction of $[Ag_{eff}]$ was accounted for dissolved Ag_{eff} (11% to 15%) in both reactors in Phase III compared to Phases I and II (Figure 1C). Attached biofilm retained less than 20% of cumulative $M_{Ag_{inf}}$ in $MBBR_1$ (1.52 mg Ag/m^2 of carrier active surface) and $MBBR_2$ (15.2 mg Ag/m^2 of carrier active surface), respectively, and significant fraction of cumulative $M_{Ag_{inf}}$ (> 78%) was released via the effluent of the both reactors by the end of Phase III (day 189; Figure 1D, E), indicating poor retention

capacity of the biofilm over long term exposure. Similar high bioaccumulation of AgNPs[11] and silica-coated iron oxide[35] in wastewater biofilms were reported at low NP concentrations over short-term exposure whereas detachment of NP-rich biofilms became a source of NP-release as NP concentrations increased over time.

A general conclusion from previous studies conducted in batch experiments[36], sequencing batch reactors[7], membrane bioreactors[37] and municipal WRRFs[4] indicated an efficient AgNP removal (72% to 95%) via accumulation in suspended growth activated sludge processes with no extensive AgNP washout as shown here for the MBBRs. The quantitative characterization of nanoparticles in MBBRs, using spICP-MS, indicated an initial adaptation of MBBR to silver addition with an increase in total Ag release over time, predominantly in NP form, and a periodic silver accumulation in biofilm coupled with a biomass concentration increase (Figure S4). Our results imply that there is a limited retention capacity of aerobic heterotrophic biofilm for AgNPs over a long time exposure, compared to the commonly studied activated sludge systems. The observed decrease in $[\text{dissolved Ag}_{\text{eff}}]$ over time in both MBBRs can be attributed to the removal of Ag^{+} via their interaction with functional groups of macromolecules such as cysteine and methionine in the EPS and biofilm matrix and their organic ligands, such as thiols[38,39,40]. Complete inhibition or significant decrease of AgNPs dissolution was reported in the presence of Cl^{-} ions at low Cl/Ag ratios[39]. We detected similar changes in the chemical composition of the particles in the effluent of the MBBRs using TEM-EDS analysis (Figure S2). Similar complexation of dissolved silver in wastewater effluents and their significantly reduced bioavailability were reported for a 7 day-experiment[40]. Azodi et al.[23] attributed the decrease in dissolved Ag concentrations in the wastewater effluent to the reformation of the secondary NPs from dissolved Ag.

259

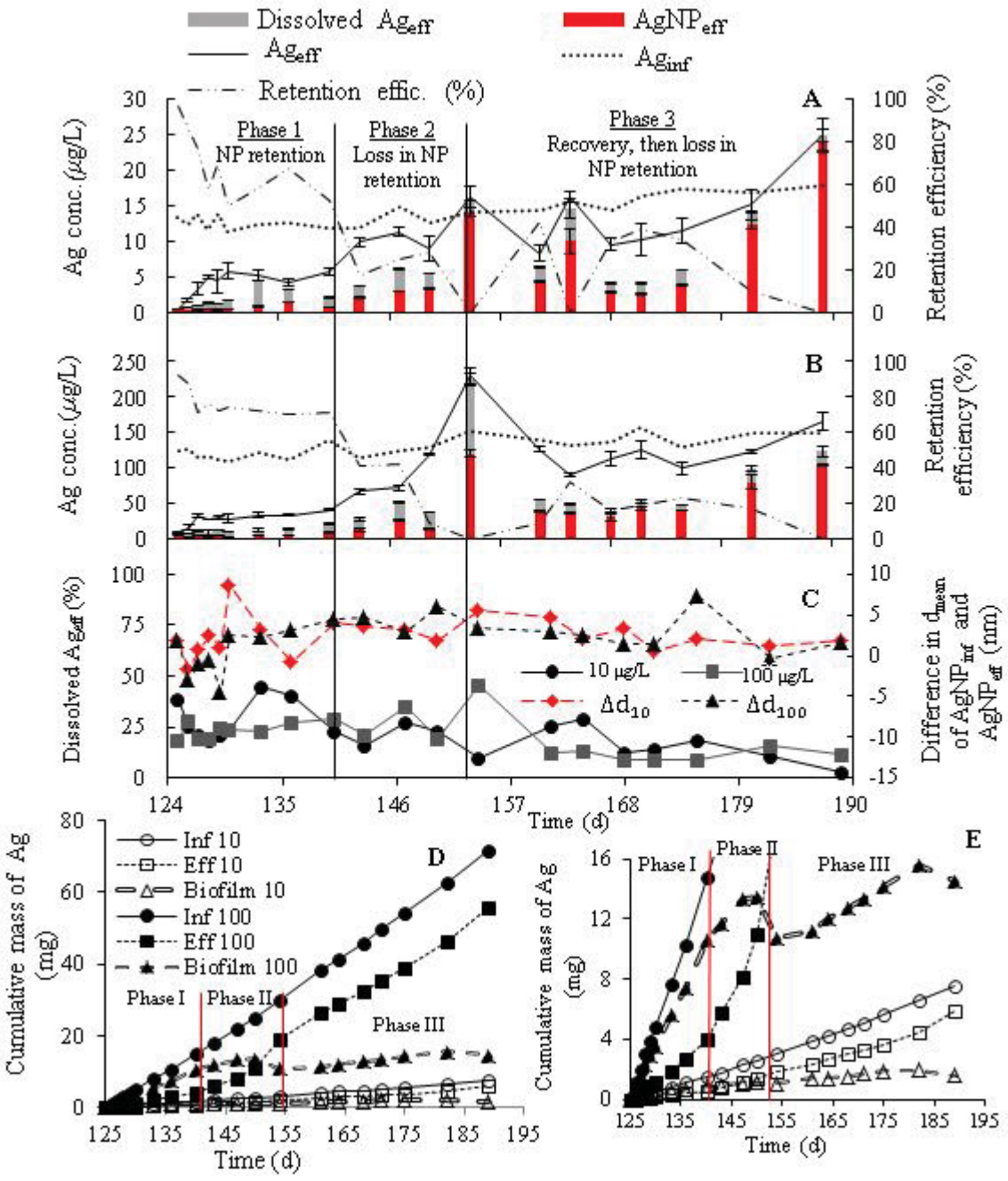

260

261 **Figure 1.** Fate and retention of Ag in MBBR receiving influent concentration of (A) 10 μg/L
262 AgNPs and (B) 100 μg/L AgNPs, (C) dissolution of $AgNP_{eff}$ (%) and difference in mead
263 diameter (d_{mean}) of $AgNP_{inf}$ and $AgNP_{eff}$, (D) cumulative Ag mass distribution in influent (Inf),
264 attached biofilm (Biofilm) and effluent (Eff) and (E) enlarged Y-scale of panel D.

265

3.2 Effects of AgNPs on the biological performance of a heterotrophic aerobic biofilm

The biofilm-mediated S_{COD} removal efficiency was determined in the two MBBRs in response to the 64-day continuous exposure to $[AgNP_{inf}]$ of 10.9 and 109 μg/L (Figure 2A, B). Prior to exposure to the AgNPs, both reactors consisted of 98% ± 0.2% viable biofilm over the control period (day 90-124) (Figure 3A) which stabilized the S_{COD} removal efficiency at 93% under quasi steady state conditions (Figure 2A-C). The biodegradation of S_{COD} remained stable, after injection of AgNPs, with an average S_{COD} removal efficiency of 92% ± 0.7% over the first 35 days (day 125-161) in $MBBR_1$ and 91% ± 2% over 23 days (day 125-147) in $MBBR_2$ indicating an unperturbed primary phase (Figure 2C) with relatively stable biofilm viability (> 96%) (Figure 3A). Measured AgNP concentrations in $MBBR_1$ (0.16 to 0.60 μg/L $AgNP_{bio}$) and $MBBR_2$ (0.7 to 5.02 μg/L $AgNP_{bio}$) and their corresponding $\text{dissolved } Ag_{bio}$ of 0.3 to 1.2 μg/L and 1.5 to 8.4 μg/L, respectively, over Phase I (Figure S2) were much lower than previously reported threshold concentrations for toxicity of AgNPs and dissolved Ag for biofilms ($IC_{50,\ PVP\text{-}AgNP@48h}$ = 114 μg/L and $IC_{50,Ag+@48h}$ = 44 μg/L[41]). As AgNP concentrations increased in reactors (Figure S2C, D), a secondary phase was observed with higher numbers of inactivated cells, resulting in significant inhibition of viable attached biofilm in $MBBR_1$ (8%) and $MBBR_2$ (31%) by day 189 (Figure 3A). The S_{COD} removal efficiency significantly decreased ($p < 0.05$) by about 11% over 29 days (day 160-189) in $MBBR_1$, and by 31% after 41 days (day 133-189) in $MBBR_2$ (Figure 2C), corresponding to the observed patterns in Ag_{bio} and Ag_{eff} time profiles. Exposure to both $AgNP_{inf}$ concentrations also induced biofilm detachment from the surface of the carriers, corresponding to the significant increase of TSS_{eff} (Figure S5). Significant detachment of wastewater biofilm and concurrent release of accumulated AgNPs were similarly reported at environmentally relevant AgNPs concentrations (22 and 105 μg/L AgNPs)[11].

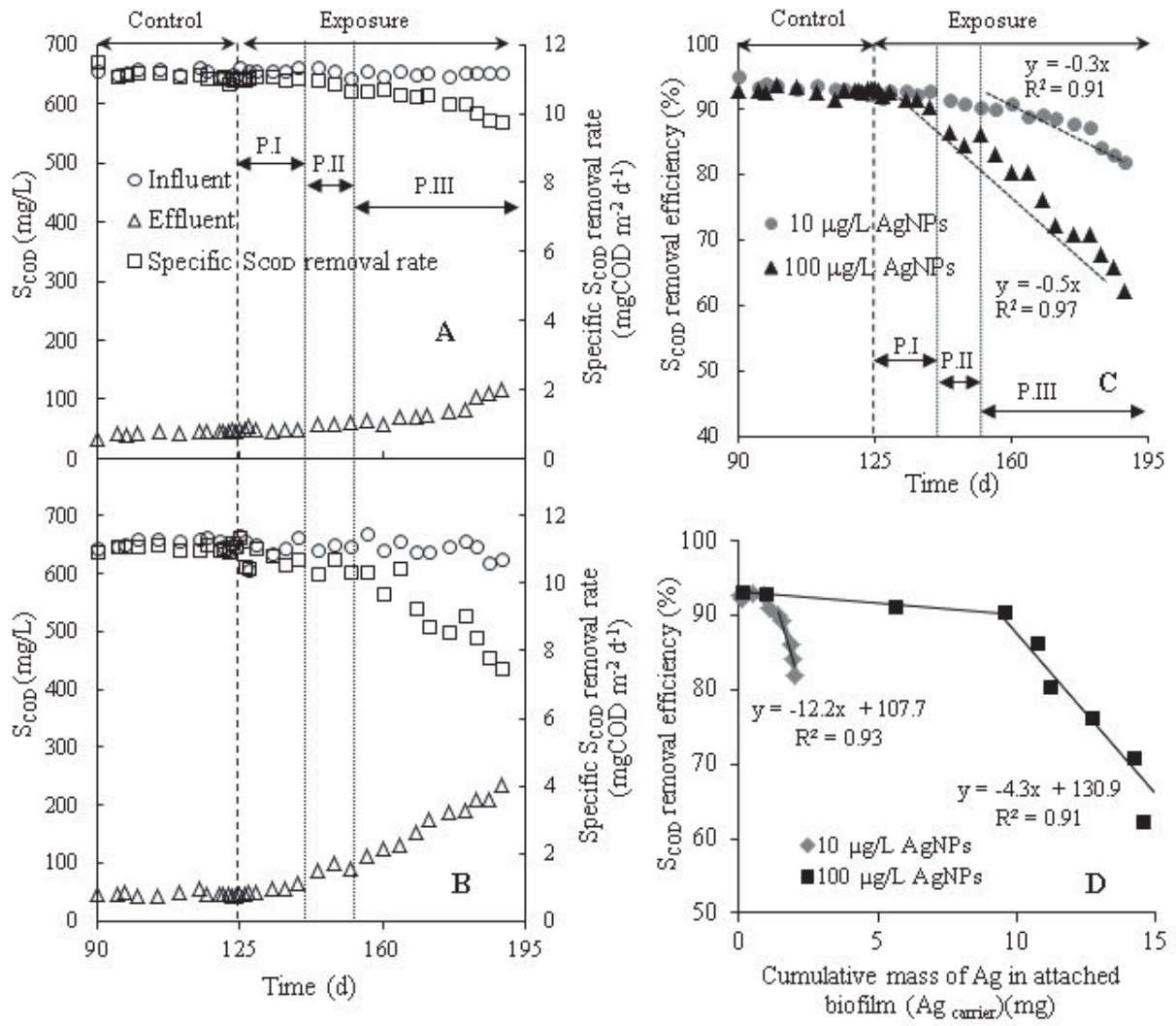

Figure 2. Effect of PVP-AgNPs addition on MBBR performance at (A) 10 μg/L AgNPs (B) 100 μg/L AgNPs, (C) S_{COD} removal efficiency and (D) correlation between $Ag_{carrier}$ and S_{COD} removal efficiency (error bars are only shown when larger than symbol size). Note: P.I-III refers to three observed phases in Ag distribution profile.

The inhibitory effect of AgNPs on both the S_{COD} removal efficiency (Figure 2D) and the biofilm viability inhibition (Figure 3B) were highly correlated ($0.91 < R^2 < 0.97$) to the retained mass of Ag in the carriers ($Ag_{carrier}$). High biomass surface area/volume ratio in attached growth processes (e.g. MBBR) enhances the deposition rate of AgNPs to attached biomass over time, leading to enhanced Ag retention per unit weight of biomass in MBBR. Thus, significant accumulation and associated mass transport of AgNPs into deeper layers of the biofilm can lead

to extensive spatial distribution of AgNPs in the biofilm cells, delivering toxic Ag^+ directly to adherent cells via interfacial dissolution of the surface-bound AgNPs and/or partly via direct uptake, leading to an enhanced time exposure and greater toxicity[42].

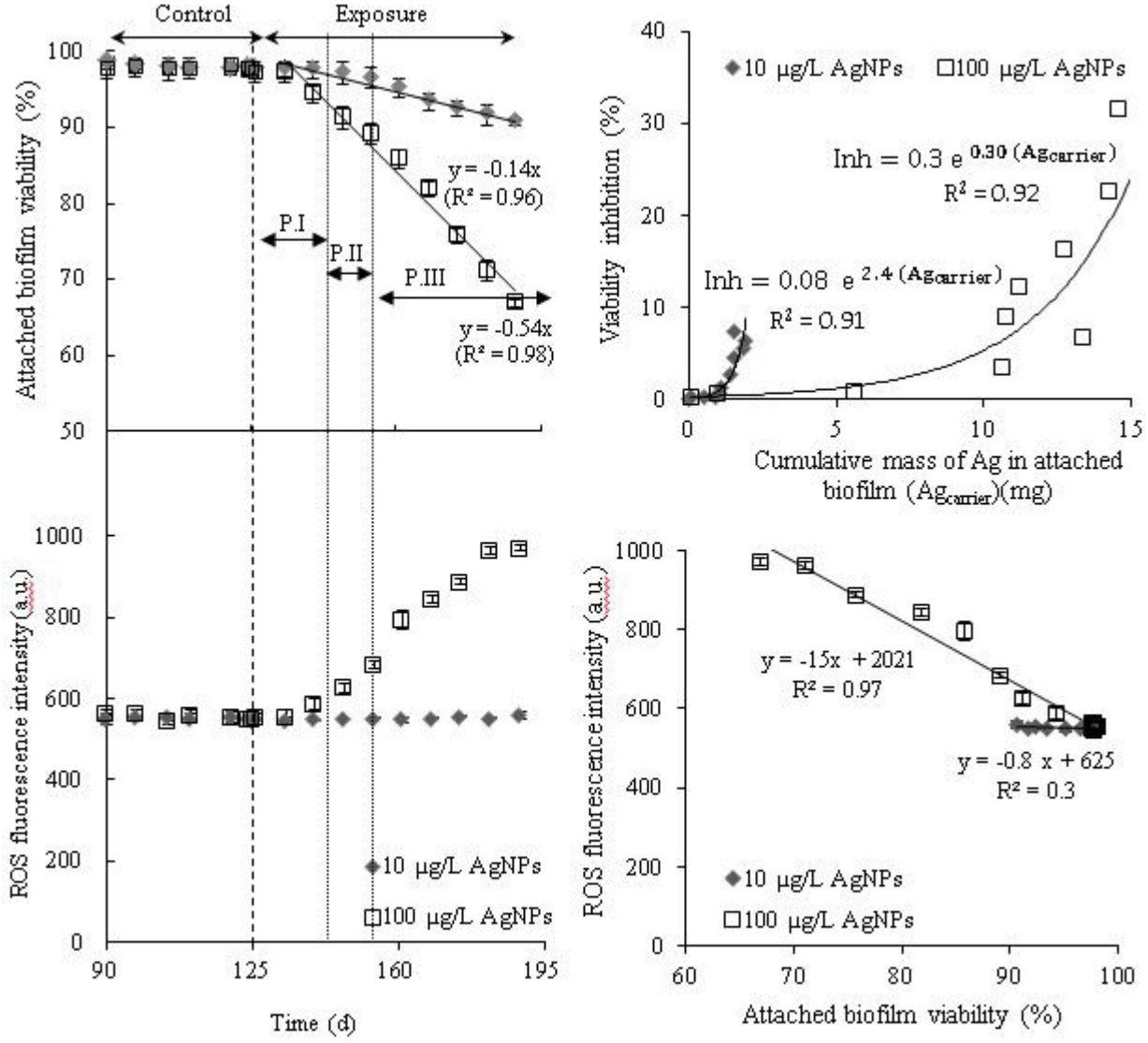

Figure 3. Effect of continuous PVP-AgNP injection on (A) attached cell viability, (B) intracellular ROS generation, (C) correlation between $Ag_{carrier}$ and attached biofilm viability inhibition and (D) correlation between viability inhibition and intracellular ROS generation (error bars are only shown when larger than symbol size). Note: P.I-III refers to three observed phases in Ag distribution profile.

Intracellular ROS did not significantly change in $MBBR_1$ (10.9 μg/L $AgNP_{inf}$), whereas its concentration increased significantly (1.78-fold, $p < 0.05$) in $MBBR_2$ (109 μg/L $AgNP_{inf}$) over 64 days (Figure 2C), consistent with reported concentration-dependent ROS production in activated sludge[32]. No correlation between biofilm viability inhibition and ROS production was observed in $MBBR_1$ whereas the cell membrane integrity damage was highly correlated to increased ROS generation in $MBBR_2$ ($R^2 = 0.97$) (Figure 3D), indicating both ROS-mediated and ROS-independent effects of AgNPs on cell membrane integrity[32]. The interaction between AgNPs/Ag^+ and the functional groups of proteins, involved in the cell respiratory chain, can lead to intracellular ROS production. Biofilm was able to regulate the ROS production at lower AgNP concentrations (1.4 to 9.04 μg/L $AgNP_{bio}$), likely via ROS scavenging enzymes (e.g. superoxide dismutase) [43], higher concentrations of AgNPs in $MBBR_2$ (10.3 to 46.2 μg/L $AgNP_{bio}$), however, caused significant overproduction of ROS which can overwhelm the antioxidant systems and induce oxidative damage to cell membranes by for example modification of the unsaturated fatty acids of the membrane phospholipids[44].

3.3 Inhibitory effect of AgNPs on key enzymatic activities of aerobic heterotrophic biofilm

Average DHA specific activity was inhibited by about 11% and 27% in $MBBR_1$ and $MBBR_2$, respectively, after 64 days (Figure $4A_1$). The specific activity of α-Glu and PRO were reduced by 16% ± 2% and 8% ± 1%, respectively, in $MBBR_1$. Higher enzyme activity inhibitions, up to 39% ± 2% (α-Glu) and 18% ± 2% (PRO), were observed at higher [$AgNP_{inf}$] in $MBBR_2$ (Figure $4B_1$, C_1), indicating a dose-dependent effect of AgNPs on specific enzymatic activities of biofilms[45,486]. Significantly different inhibition rates and half-lives of all three enzymes upon exposure to AgNPs (Table S4) indicated the distinct sensitivity of these enzymes to AgNPs due to their different properties and location patterns in the biofilm matrix[47].

345 The inhibitory effects of AgNPs on specific enzymatic activities of biofilm was highly correlated
346 ($0.80 < R^2 < 0.96$) to the retained mass of Ag in the carriers ($Ag_{carrier}$) (Figure $4A_2$-C_2). The
347 observed pattern highlights the major role of diffusion of retained AgNPs in the biofilm-laden
348 system upon the targeted delivery of both AgNPs and dissolved Ag in close proximity of
349 enzymes and possibly inside the cell in order to reach the Ag concentration needed to exceed
350 inhibitory limits.

351 Upon the initial contact with enzymes in the biological media, nanoparticles acquire a protein
352 corona leading to substantial structural changes of the enzyme[48]. Extracellular enzymes (e.g. α-
353 Glu) interact initially via their functional groups (e.g. carboxyl, hydroxyl, amine, amido, keto)
354 with both the ring and polyvinyl domain of PVP coating and the oxygen atom involved in PVP-
355 nanoparticle complex form. The strong bonding of AgNPs and dissolved Ag with electron
356 donors containing sulfur, oxygen, or nitrogen (e.g. thiols, carboxylates, phosphates, hydroxyl,
357 amines, imidazoles, indoles) across the enzymes can form silver complexes which shield the
358 active sites and alter the enzyme's conformation or distort its 3D structure so it no longer retains
359 its full enzymatic activity[49]. Breaking through the barrier of outer membrane permeability,
360 AgNPs and dissolved Ag can strongly associate with specific sequences of amino acids on the
361 DHA active site and thiol (–SH) group of cysteine, by replacing the hydrogen atom to form –S–
362 Ag, and irreversibly inactivate dehydrogenase enzymatic functions leading to cellular respiration
363 inhibition[49,50]. Moreover, the ROS-mediated protein oxidation and microbial community
364 composition alteration can result in loss of function for enzymes associated with biofilms and in
365 a cutback in their production and secretion [47].

366

367

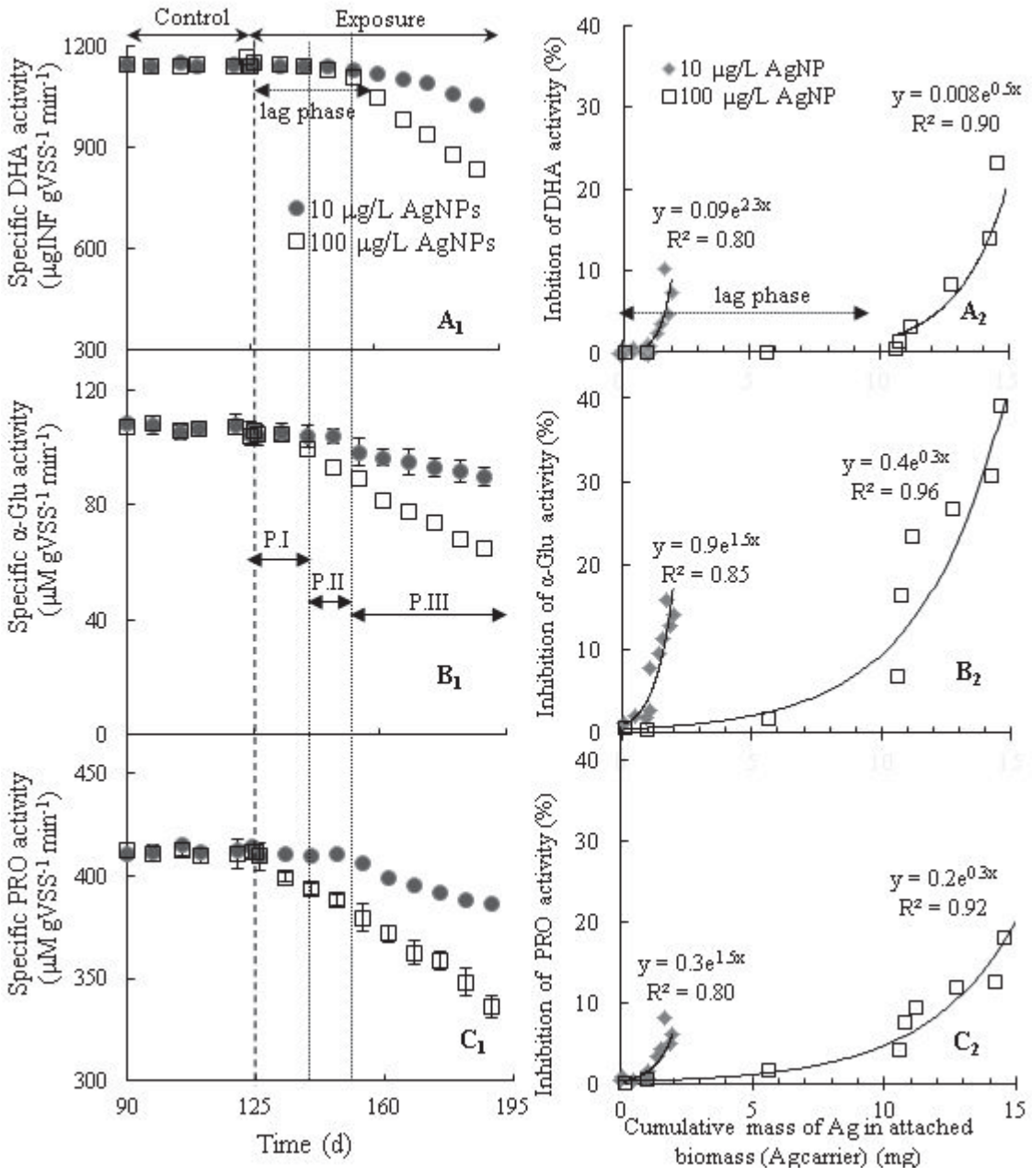

368

369 **Figure 4.** Effect of continuous PVP-AgNP injection on specific activity of (A_1) DHA (B_1) α-Glu
370 and (C_1) PRO, (A_2-C_2) correlation between $Ag_{carrier}$ and enzyme activity inhibition (Error bars
371 are only shown when larger than symbol size).

372

373 **3.4 Effects of AgNPs on the microbial community of the heterotrophic wastewater biofilm**

374 Seven major phyla *(Proteobacteria*, *Bacteroidetes*, *Verrucomicrobia*, *Gemmatimonadetes*
375 *Planctomycetes*, *Actinobacteria*) were identified (abundance > 1%) at the end of the control

period in both reactors ($MBBR_1^C$, $MBBR_2^C$) (Figure 5A), as previously reported in microbial composition wastewater biofilm studies[51,52]. *Proteobacteria* was the most abundant phylum majorly comprised of *Alphaproteobacteria*, *Betaproteobacteria* and *Gammaproteobacteria*. Certain phyla demonstrated a distinct behavior at two [$AgNP_{inf}$] after 64 days of exposure (day 189). The relative abundance of *Proteobacteria* decreased at lower doses of AgNPs ($MBBR_1^{64}$) but increased at the higher dose of AgNPs ($MBBR_2^{64}$) in contrast to *Verrucomicrobia* (Figure 5A). AgNPs influenced biofilm microbial phylum abundance in a dose-dependent manner, which was confirmed by the principal coordinate analysis (PCoA) based on the weighted UniFrac distance matrix with 75% of total variance on PCoA1 axis (Figure S6). The observed pattern indicated various responses among taxa, including a range from susceptibility towards silver (*e.g. Bacteroidetes* and *Gemmatimonadetes)* to tolerance against silver (*e.g.Planctomycetes)*, as reported in previous studies[53,54].

The heatmap of genera, with total sequence reads higher than 150 in selected phyla, showed the distinct sensitivity of certain genera at both [$AgNP_{inf}$] (Figure 5B). The relative abundance of *Rhodobacter,* identified as the most abundant OTU at the genus level (*Rhodobacteraceae*, *α-proteobacteria*) decreased in both reactors. Higher abundance of *Paracoccus* other dominant genera from the *Rhodobacteraceae* family and *Zooglea* (*ß-proteobacteria*) at higher [$AgNP_{inf}$], is likely associated with their heavy metal resistance to enhance their survival in metal-contaminated environments[55]. The abundance of *Sphingomonas* genus (*Sphingomonadaceae)* decreased in $MBBR_1^{64}$ whereas its abundance increased in $MBBR_2^{64}$, possibly due to the presence of signaling molecules (e.g. sphingolipids) in their outer membrane maintaining community diversity at higher silver concentrations[56]. The genera affiliated with *Xanthomonadaceae* family such as *Stenotrophomona* (*ɣ-proteobacteria*) are reported as N-acyl-

399 homoserine-lactone (AHL) producers in aerobic granular sludge and biofilm, contributing to
400 AHL-mediated quorum sensing signaling, integrity and biofilm stability[57]. Thus, the reduction in
401 their relative abundance at both [$AgNP_{inf}$] affected both COD removal efficiency and integrity of
402 biofilm structures.

403 Chronic exposure to both [$AgNP_{inf}$] greatly decreased the relative abundance of genera affiliated
404 to three dominant orders in the *Bacteroidetes* phylum (*Sphingobacteriales*, *Flavobacteriales*,
405 *Cytophagales*) known as the core members of microbial communities in WRRFs degrading
406 complex organic materials[58], resulting in reduced abundance of *Bacteroidetes* and a correlated
407 lower COD removal efficiency in both reactors. Similar differential susceptibilities to AgNPs
408 were observed in other identified phyla with a shift towards silver-tolerant genera (e.g.
409 *Gemmata*) or more sensitive genera (e.g *Gemmatimonas)*. Although the alpha diversity of the
410 bacterial community was not significantly impacted (Table S4), the bacterial community
411 composition was clearly changed, as shown in Figure 5B, due to a decrease or loss of silver-
412 sensitive species in certain orders (e.g. *Burkholderiale* or *Gemmatimonadales*). The observed
413 shift in the microbial community composition can trigger a potential impairment of the biofilm
414 biological functions pertaining to organic matter biodegradation, enzymatic activities and biofilm
415 structural properties.

416

417

418

419

420

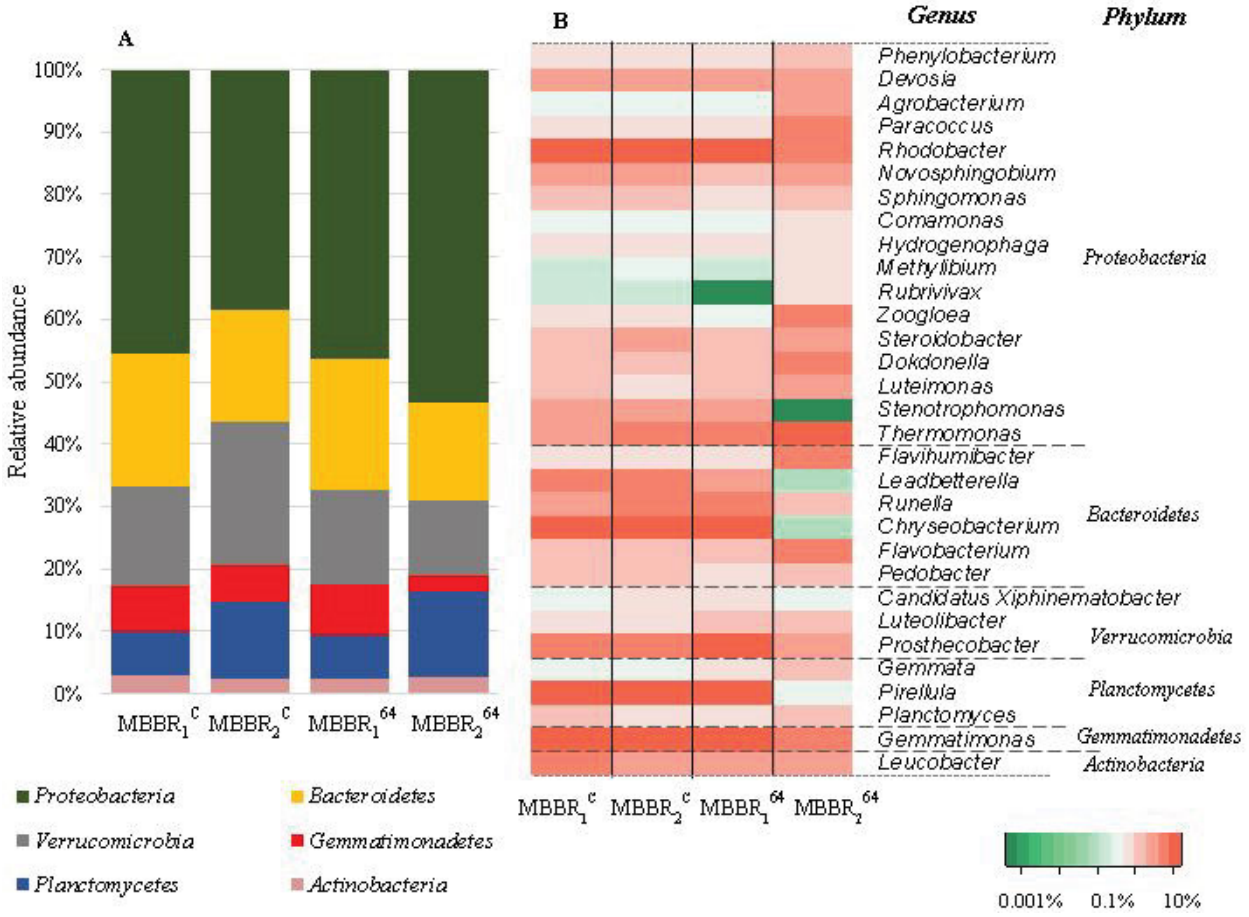

Figure 5. (A) Taxonomic classification of 16S rDNA paired-end sequencing from the biofilm samples at different AgNP concentrations at phylum level and (B) heatmap of genera with total sequence reads higher than 150 in selected phyla. Note: Superscripts C and 64 represent the biofilms collected at the end of control period and after 64 days of AgNPs exposure in MBBRs, respectively.

4. Environmental implications

The MBBR technology has been successfully used for the treatment of many types of wastewaters from municipalities, paper mills, pharmaceutical industries and fish farms[59]. MBBRs can be easily combined with other pre- or post- treatment technologies such as settling and membrane separation, or used in a series of aerobic and anaerobic MBBRs, thus increasing the likelihood of achieving a 'zero discharge' goal[60]. Our findings, however, suggests that the

extended release of AgNPs and Ag-rich biofilm from an MBBR can exert a strong effect on downstream treatments that may lead to membrane fouling, for example, due to significant biofilm detachment, or to potential risks in effluent receiving streams that could impact ecosystems. Our results, corroborated with previous studies[18,52], signify that short-term exposure tests may underestimate the inhibitory effects of AgNPs in biofilm-laden environments, especially for treatment processes with long sludge retention times where long-term continuous exposure to AgNPs can result in a cumulative effect of NP-biofilm interaction dynamics leading to a different level of NP-mediated susceptibility in the biofilm. For example, there was no sulfidation of AgNPs in these MBBRs deployed here, due to lack of sulfur in the synthetic wastewater. Sulfidation of AgNPs has been shown to retard dissolution of AgNP due to formation of Ag_2S and organosulfur complexes and could have displayed less[23, 61].

ASSOCIATED CONTENT

Supporting Information

Additional information is provided for synthetic wastewater composition (Table S1-2) and reactor operational conditions, characterization of biofilm biological responses, intracellular ROS measurements, sp-ICP-MS instrumentation (Table S3) and TEM-EDS, cumulative total Ag mass balance calculations, biofilm enzyme's half-life and inhibition rates (Table S4), richness and diversity of microbial communities of biofilm (Table S5). In addition, fractionation of Ag in reactor components are provided (Figure S1), $Ag_{inf/bio}$ time distribution (Figure S2), $AgNP_{inf/eff}$ particle size distribution (Figure S3), TEM images and EDS analysis for $AgNP_{inf/eff}$ (Figure S4), effluent TSS profile (Figure S5) and principal coordinate analysis (Figure S6) and additional discussion on microbial community analysis.

Acknowledgements

The authors thank the Natural Sciences and Engineering Research Council of Canada (Grant no. STPGP 430659–12), Environment and Climate Change Canada, PerkinElmer, Health Sciences Canada, the Fonds de Recherche du Québec Nature et Technologies (FRQNT), the Canadian Water Network (CWN), SNC Lavalin Environment, the City of Calgary and the City of Saint-Hyacinthe for their financial support. The authors thank Jean-Philippe Massé, Le Centre de Caractérisation Microscopique des Matériaux of Polytechnique Montreal for TEM/EDS analysis, and Jean-Baptiste Burnet for DNA extraction and the Terrebonne/Mascouche WRRF for assistance with wastewater sampling.

References

1. Vance, M. E.; Kuiken, T.; Vejerano, E. P.; McGinnis, S. P.; Hochella Jr, M. F.; Rejeski, D.; Hull, M. S., Nanotechnology in the real world: Redeveloping the nanomaterial consumer products inventory. *Beilstein J. Nanotechnol.* **2015,** *6*, 1769.
2. Gottschalk, F.; Sonderer, T.; Scholz, R. W.; Nowack, B., Modeled environmental concentrations of engineered nanomaterials (TiO_2, ZnO, Ag, CNT, fullerenes) for different regions. *Environ. Sci. Technol.* **2009**, 43, (24), 9216-9222.
3. Keller, A. A.; Lazareva, A., Predicted releases of engineered nanomaterials: From global to regional to local. *Environ. Sci. Technol. Let.* **2013,** *1*, (1), 65-70.
4. Li, L.; Hartmann, G.; Döblinger, M.; Schuster, M., Quantification of nanoscale silver particles removal and release from municipal wastewater treatment plants in Germany. *Environ. Sci. Technol.* **2013,** *47*, (13), 7317-7323.
5. Alito, C. L.; Gunsch, C. K., Assessing the effects of silver nanoparticles on biological nutrient removal in bench-scale activated sludge sequencing batch reactors. *Environ. Sci. Technol.* **2014,** *48*, (2), 970-976.
6. Yuan, Z.-H.; Yang, X.; Hu, A.; Yu, C.-P., Long-term impacts of silver nanoparticles in an anaerobic–anoxic–oxic membrane bioreactor system. *Chem. Eng. J.* **2015,** *276*, 83-90.
7. Zhang, Z.; Gao, P.; Li, M.; Cheng, J.; Liu, W.; Feng, Y., Influence of silver nanoparticles on nutrient removal and microbial communities in SBR process after long-term exposure. *Sci. Total Environ.* **2016,** *569*, 234-243.
8. Liang, Z.; Das, A.; Hu, Z., Bacterial response to a shock load of nanosilver in an activated sludge treatment system. *Water Res.* **2010,** *44*, (18), 5432-5438.
9. Sheng, Z.; Van Nostrand, J. D.; Zhou, J.; Liu, Y., Contradictory effects of silver nanoparticles on activated sludge wastewater treatment. *J.Hazard. Mater.* **2018,** *341*, 448-456.
10. Falletti, L.; Conte, L., Upgrading of activated sludge wastewater treatment plants with hybrid moving-bed biofilm reactors. *Ind. Eng. Chem. Res.* **2007,** *46*, (21), 6656-6660.
11. Walden, C.; Zhang, W., Bioaccumulation of silver nanoparticles in model wastewater biofilms. *Environ. Sci.: Water Res. Technol.* **2018**.
12. Borkar, R.; Gulhane, M.; Kotangale, A., Moving bed biofilm reactor–a new perspective in wastewater treatment.. *Toxicology and Food Technology* **2013,** *6*, (6), 15-21.
13. Biswas, K.; Taylor, M. W.; Turner, S. J., Successional development of biofilms in moving bed biofilm reactor (MBBR) systems treating municipal wastewater. *Appl. Microbiol. Biot.* **2014,** *98*, (3), 1429-1440.
14. Fabrega, J.; Renshaw, J. C.; Lead, J. R., Interactions of silver nanoparticles with *Pseudomonas putida* biofilms. *Environ. Sci. Technol.* **2009,** *43*, (23), 9004-9009.
15. Fabrega, J.; Zhang, R.; Renshaw, J. C.; Liu, W.-T.; Lead, J. R., Impact of silver nanoparticles on natural marine biofilm bacteria. *Chemosphere* **2011,** *85*, (6), 961-966.
16. Mallevre, F.; Fernandes, T. F.; Aspray, T. J., *Pseudomonas putida* biofilm dynamics following a single pulse of silver nanoparticles. *Chemosphere* **2016,** *153*, 356-364.
17. Peulen, T.-O.; Wilkinson, K. J., Diffusion of nanoparticles in a biofilm. *Environ. Sci. Technol.* **2011,** *45*, (8), 3367-3373.

18. Barker, L.; Giska, J.; Radniecki, T.; Semprini, L., Effects of short-and long-term exposure of silver nanoparticles and silver ions to *Nitrosomonas europaea* biofilms and planktonic cells. *Chemosphere* **2018,** *206*, 606-614.
19. Alizadeh, S.; Ghoshal, S.; Comeau, Y., Fate and inhibitory effect of silver nanoparticles in high rate moving bed biofilm reactors. *Sci. Total Environ.* **2019,** *647*, 1199-1210.
20. Walden, C.; Zhang, W., Biofilms versus activated sludge: considerations in metal and metal oxide nanoparticle removal from wastewater. *Environ. Sci. Technol.* **2016,** *50*, (16), 8417-8431.
21. Merrifield, R. C.; Stephan, C.; Lead, J., Determining the concentration dependent transformations of Ag nanoparticles in complex media: Using SP-ICP-MS and Au@ Ag core–shell nanoparticles as tracers. *Environ. Sci. Technol.* **2017,** *51*, (6), 3206-3213.
22. Vidmar, J.; Oprčkal, P.; Milačič, R.; Mladenovič, A.; Ščančar, J., Investigation of the behaviour of zero-valent iron nanoparticles and their interactions with Cd^{2+} in wastewater by single particle ICP-MS. *Sci. Total Environ.* **2018,** *634*, 1259-1268.
23. Azodi, M.; Sultan, Y.; Ghoshal, S., Dissolution behavior of silver nanoparticles and formation of secondary silver nanoparticles in municipal wastewater by single-particle ICP-MS. *Environ. Sci. Technol.* **2016,** *50*, (24), 13318-13327.
24. Mitrano, D. M.; Barber, A.; Bednar, A.; Westerhoff, P.; Higgins, C. P.; Ranville, J. F., Silver nanoparticle characterization using single particle ICP-MS (SP-ICP-MS) and asymmetrical flow field flow fractionation ICP-MS (AF4-ICP-MS). *J. Anal. Atom. Spectrom* **. 2012,** *27*, (7), 1131-1142.
25. Pace, H. E.; Rogers, N. J.; Jarolimek, C.; Coleman, V. A.; Gray, E. P.; Higgins, C. P.; Ranville, J. F., Single particle inductively coupled plasma-mass spectrometry: a performance evaluation and method comparison in the determination of nanoparticle size. *Environ. Sci. Technol.* **2012,** *46*, (22), 12272-12280.
26. Giese, B.; Klaessig, F.; Park, B.; Kaegi, R.; Steinfeldt, M.; Wigger, H.; Gleich, A.; Gottschalk, F., Risks, release and concentrations of engineered nanomaterial in the environment. *Sci. Rep.* **2018,** *8*, (1), 1565.
27. Metcalf & Eddy-AECOM, Wastewater Engineering: Treatment and Resource Recovery. 5th ed., McGraw-Hill, New York, **2014.**
28. APHA; AWWA; WEF. Standard Methods for the Examination of Water and Wastewater, 22nd ed. American Public Health Association, American Water Works Association & Water Environment Federation: Washington, D.C. **2012.**
29. Chen, Y.; Chen, H.; Zheng, X.; Mu, H., The impacts of silver nanoparticles and silver ions on wastewater biological phosphorous removal and the mechanisms. *J. Hazard. Mater.* **2012,** *239*, 88-94.
30. Von Mersi, W.; Schinner, F., An improved and accurate method for determining the dehydrogenase activity of soils with iodonitrotetrazolium chloride. *Biol. Fert. Soils* **1991,** *11*, (3), 216-220.
31. Goel, R.; Mino, T.; Satoh, H.; Matsuo, T., Enzyme activities under anaerobic and aerobic conditions in activated sludge sequencing batch reactor. *Water Res.* **1998,** *32*, (7), 2081-2088.

32. Gu, L.; Li, Q.; Quan, X.; Cen, Y.; Jiang, X., Comparison of nanosilver removal by flocculent and granular sludge and short-and long-term inhibition impacts. *Water Res.* **2014,** *58*, 62-70.
33. Callahan, B. J.; McMurdie, P. J.; Rosen, M. J.; Han, A. W.; Johnson, A. J.; Holmes, S. P., DADA2: High-resolution sample inference from Illumina amplicon data. *Nat. Methods* **2016,** *13*, (7), 581-3.
34. Lin, S.; Cheng, Y.; Liu, J.; Wiesner, M. R., Polymeric coatings on silver nanoparticles hinder autoaggregation but enhance attachment to uncoated surfaces. *Langmuir* **2012,** *28*, (9), 4178-4186.
35. Herrling, M. P.; Lackner, S.; Tatti, O.; Guthausen, G.; Delay, M.; Franzreb, M.; Horn, H., Short and long term biosorption of silica-coated iron oxide nanoparticles in heterotrophic biofilms. *Sci. Total Environ.* **2016,** *544*, 722-729.
36. Kaegi, R.; Voegelin, A.; Ort, C.; Sinnet, B.; Thalmann, B.; Krismer, J.; Hagendorfer, H.; Elumelu, M.; Mueller, E., Fate and transformation of silver nanoparticles in urban wastewater systems. *Water Res.* **2013,** *47*, (12), 3866-3877.
37. Zhang, C.; Liang, Z.; Hu, Z., Bacterial response to a continuous long-term exposure of silver nanoparticles at sub-ppm silver concentrations in a membrane bioreactor activated sludge system. *Water Res.* **2014,** *50*, 350-358.
38. Gondikas, A. P.; Morris, A.; Reinsch, B. C.; Marinakos, S. M.; Lowry, G. V.; Hsu-Kim, H., Cysteine-induced modifications of zero-valent silver nanomaterials: implications for particle surface chemistry, aggregation, dissolution, and silver speciation. *Environ. Sci. Technol.* **2012,** *46*, (13), 7037-7045.
39. Ho, C. M.; Yau, S. K. W.; Lok, C. N.; So, M. H.; Che, C. M., Oxidative dissolution of silver nanoparticles by biologically relevant oxidants: a kinetic and mechanistic study. *Chemistry–An Asian Journal* **2010,** *5*, (2), 285-293.
40. Azimzada, A.; Tufenkji, N.; Wilkinson, K. J., Transformations of silver nanoparticles in wastewater effluents: links to Ag bioavailability. *Environ. Sci.: Nano* **2017,** *4*, (6), 1339-1349.
41. Yang, Y.; Alvarez, P. J., Sublethal concentrations of silver nanoparticles stimulate biofilm development. *Environ. Sci. Technol. Let.* **2015,** *2*, (8), 221-226.
42. Hsiao, I.-L.; Hsieh, Y.-K.; Wang, C.-F.; Chen, I.-C.; Huang, Y.-J., Trojan-horse mechanism in the cellular uptake of silver nanoparticles verified by direct intra-and extracellular silver speciation analysis. *Environ. Sci. Technol.* **2015,** *49*, (6), 3813-3821.
43. Abdal Dayem, A.; Hossain, M. K.; Lee, S. B.; Kim, K.; Saha, S. K.; Yang, G.-M.; Choi, H. Y.; Cho, S.-G., The role of reactive oxygen species (ROS) in the biological activities of metallic nanoparticles. *Int. J. Mol. Sci.* **2017,** *18*, (1), 120.
44. Birben, E.; Sahiner, U. M.; Sackesen, C.; Erzurum, S.; Kalayci, O., Oxidative stress and antioxidant defense. *World Allergy Organization Journal* **2012,** *5*, (1), 9.
45. Asadishad, B.; Chahal, S.; Akbari, A.; Cianciarelli, V.; Azodi, M.; Ghoshal, S.; Tufenkji, N., Amendment of agricultural soil with metal nanoparticles: Effects on soil Enzyme activity and microbial community composition. *Environ. Sci. Technol.* **2018***, 52(4),* 1908-1918.
46. Xu, Q.; Li, S.; Wan, Y.; Wang, S.; Ma, B.; She, Z.; Guo, L.; Gao, M.; Zhao, Y.; Jin, C., Impacts of silver nanoparticles on performance and microbial community and

601 enzymatic activity of a sequencing batch reactor. *J.Environ.Manage.* **2017,** *204*, 667-
602 673.
603 47. Schug, H.; Isaacson, C. W.; Sigg, L.; Ammann, A. A.; Schirmer, K., Effect of TiO_2
604 nanoparticles and UV radiation on extracellular enzyme activity of intact heterotrophic
605 biofilms. *Environ. Sci. Technol.* **2014,** *48*, (19), 11620-11628.
606 48. Ahlberg, S.; Antonopulos, A.; Diendorf, J.; Dringen, R.; Epple, M.; Flöck, R.;
607 Goedecke, W.; Graf, C.; Haberl, N.; Helmlinger, J., PVP-coated, negatively charged
608 silver nanoparticles: A multi-center study of their physicochemical characteristics, cell
609 culture and in vivo experiments. *Beilstein J. Nanotech.* **2014,** *5*, 1944.
610 49. Wigginton, N. S.; De Titta, A.; Piccapietra, F.; Dobias, J.; Nesatyy, V.; Suter, M. J.;
611 Bernier-Latmani, R., Binding of silver nanoparticles to bacterial proteins depends on
612 surface modifications and inhibits enzymatic activity. *Environ. Sci. Technol.* **2010,**
613 *44*(6), 2163-2168.
614 50. Kim, J. Y.; Lee, C.; Cho, M.; Yoon, J., Enhanced inactivation of *E. coli* and MS-2
615 phage by silver ions combined with UV-A and visible light irradiation. *Water Res.*
616 **2008,** *42*, (1), 356-362.
617 51. Miao, L.; Wang, C.; Hou, J.; Wang, P.; Ao, Y.; Li, Y.; Yao, Y.; Lv, B.; Yang, Y.;
618 You, G., Response of wastewater biofilm to CuO nanoparticle exposure in terms of
619 extracellular polymeric substances and microbial community structure. *Sci. Total*
620 *Environ.* **2017,** *579*, 588-597.
621 52. Wang, P.; You, G.; Hou, J.; Wang, C.; Xu, Y.; Miao, L.; Feng, T.; Zhang, F.,
622 Responses of wastewater biofilms to chronic CeO_2 nanoparticles exposure: Structural,
623 physicochemical and microbial properties and potential mechanism. *Water Res.* **2018**.
624 *133*, 208-217.
625 53. Grün, A. Y.; App, C. B.; Breidenbach, A.; Meier, J.; Metreveli, G.; Schaumann, G. E.;
626 Manz, W., Effects of low dose silver nanoparticle treatment on the structure and
627 community composition of bacterial freshwater biofilms. *PloS one* **2018,** *13*, (6),
628 e0199132.
629 54. Cao, C.; Huang, J.; Yan, C.; Liu, J.; Hu, Q.; Guan, W., Shifts of system performance
630 and microbial community structure in a constructed wetland after exposing silver
631 nanoparticles. *Chemosphere* **2018,** *199*, 661-669.
632 55. Zheng, X.-y.; Lu, D.; Chen, W.; Gao, Y.-j.; Zhou, G.; Zhang, Y.; Zhou, X.; Jin, M.-Q.,
633 Response of aerobic granular sludge to the long-term presence of CuO NPs in A/O/A
634 SBRs: Nitrogen and phosphorus removal, enzymatic activity, and the microbial
635 community. *Environ. Sci. Technol.* **2017,** *51*, (18), 10503-10510.
636 56. Yang, Y.; Quensen, J.; Mathieu, J.; Wang, Q.; Wang, J.; Li, M.; Tiedje, J. M.; Alvarez,
637 P. J., Pyrosequencing reveals higher impact of silver nanoparticles than Ag^+on the
638 microbial community structure of activated sludge. *Water Res.* **2014,** *48*, 317-325.
639 57. Tan, C. H.; Koh, K. S.; Xie, C.; Tay, M.; Zhou, Y.; Williams, R.; Ng, W. J.; Rice, S.
640 A.; Kjelleberg, S., The role of quorum sensing signalling in EPS production and the
641 assembly of a sludge community into aerobic granules. *The ISME journal* **2014,** *8*, (6),
642 1186.
643 58. Chen, Y.; Zhao, Z.; Peng, Y.; Li, J.; Xiao, L.; Yang, L., Performance of a full-scale
644 modified anaerobic/anoxic/oxic process: high-throughput sequence analysis of its
645 microbial structures and their community functions. *Bioresource Technol.***2016,** *220*,
646 225-232.

59. Revilla, M.; Galán, B.; Viguri, J. R., An integrated mathematical model for chemical oxygen demand (COD) removal in moving bed biofilm reactors (MBBRs) including predation and hydrolysis. *Water Res.* **2016,** *98*, 84-97.
60. Bakar, S. N. H. A.; Hasan, H. A.; Mohammad, A. W.; Abdullah, S. R. S.; Haan, T. Y.; Ngteni, R.; Yusof, K. M. M., A review of moving-bed biofilm reactor technology for palm oil mill effluent treatment. *J.Clean. Prod.* **2018,** *171*, 1532-1545.
61. Levard, C.; Reinsch, B. C.; Michel, F. M.; Oumahi, C.; Lowry, G. V.; Brown Jr, G. E., Sulfidation processes of PVP-coated silver nanoparticles in aqueous solution: impact on dissolution rate. *Environ. Sci. Technol.* **2011**, 45, (12), 5260-5266.

TABLE OF CONTENT GRAPHIC

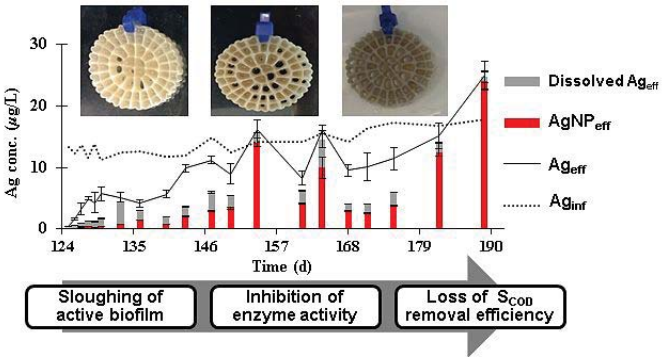

677

678

679